Periodica Polytechnica
Chemical Engineering

60(1), pp. 29-39, 2016
DOI: 10.3311/PPch.8227

Design and Preparation of CO Tolerant Anode Electrocatalysts for PEM Fuel Cells

Dorottya Gubán[1], Zoltán Pászti[1*], Irina Borbáth[1], István Bakos[1], Eszter Drotár[1], István Sajó[1], András Tompos[1]

RESEARCH ARTICLE

Received 12 May 2015; accepted after revision 24 June 2015

Abstract

In this contribution the preparation and the thorough characterization of a novel electrocatalyst support material consisting of a composite of $Ti_{0.7}W_{0.3}O_2$ mixed oxide and activated carbon is presented. A sol-gel based synthesis method optimized for depositing rutile TiO_2 with high level of isovalent tungsten incorporation onto activated carbon was elaborated and the process of tungsten incorporation was followed by XRD and in situ XPS measurements. Electron microscopy studies demonstrated that Pt loading of the support by the $NaBH_4$-assisted ethylene-glycol reduction method results in finely dispersed and highly stable nanoparticles. The assessment of the electrochemical properties of the catalyst revealed its enhanced CO tolerance and long term stability when compared to activated carbon supported Pt or state-of-art CO tolerant PtRu catalysts.

Keywords

Anode electrocatalysts, conducting Ti-W mixed oxides, composite materials, CO-tolerance, XPS, XRD

[1] Institute of Materials and Environmental Chemistry,
Research Centre for Natural Sciences,
Hungarian Academy of Sciences,
H-1117 Budapest, Magyar tudósok körútja 2, Hungary

[*] Corresponding author, e-mail: paszti.zoltan@ttk.mta.hu

1 Introduction

Fuel cells are clean and reliable energy sources, which convert the chemical energy content of hydrogen-rich fuels into electricity practically without emission of greenhouse gases. In particular, polymer electrolyte membrane (PEM) fuel cells with their high efficiency and low operation temperature are considered as ideal power sources for mobile applications ranging from handhold electronic equipments to transportation vehicles. For the wide-range implementation of PEM fuel cells it is most essential to produce low-cost durable units. A significant part of the price belongs to the electrocatalysts, which are required in high amounts with platinum as the material of choice for their active element. The use of platinum also raises questions with regard to stability, since the hydrogen fuel produced by reforming contains small amount of carbon monoxide that poisons the catalysts. In case of direct methanol fuel cells CO is one of the intermediate products of the electrooxidation reaction. In addition, the typical catalyst support, activated carbon tends to corrode under the fast load change conditions encountered frequently in fuel cells used in transportation applications, which rapidly deteriorates the performance of the catalysts [1]. Accordingly, current research on fuel cells catalysts focuses on developing stable, CO-tolerant electrocatalysts with reduced platinum content.

There are three suitable pathways in the development of such novel catalysts: (i) alloying the active noble metal (Pt) with other oxophilic metals, (ii) modification or replacement of the activated carbon support by more corrosion resistant, electrical conductive materials with high surface area, or (iii) development of noble metal free catalysts.

In this study we followed the second pathway. The stability and corrosion resistance of titanium dioxide is well known. TiO_2 is an n-type semiconductor having a wide band gap (3.0– 3.5 eV) and it has been used as a catalyst support in fuel cells, even though its electronic conductivity is much lower than that of conventional carbon supports [2-3]. However, electronic conductivity of titanium dioxide can be improved by isovalent cation substitution with tungsten [4]. High surface area TiO_2 is also capable to stabilize metal loadings in highly dispersed state, thus it is a widely used support in conventional heterogeneous catalysis.

Several examples could be found in the literature for the implementation of anode electrocatalysts modified with tungsten-oxides, since in their presence the oxidation of CO shifts towards more negative potential than in case of pure Pt [5-6]. Furthermore on account of the so called 'spill-over effect' tungsten oxides improve the catalytic activity in the hydrogen oxidation reaction as well [7]. Their application is limited by their instability due to dissolution in both alkaline and acidic conditions. The latter is particularly important, as electrocatalysts of a PEM fuel cell work in an acidic milieu. Nevertheless, the stability issue is expected to be improved by incorporating tungsten into the TiO_2 lattice.

Wang et al. [8] applied $Ti_{0.7}W_{0.3}O_2$ mixed oxide as a catalyst support. After depositing Pt onto it, it was mixed with 20 wt% activated carbon to ensure the necessary electronic conductivity. Improved CO tolerance was observed during their measurements but at the same time, due to the lower active Pt specific surface area on the $Ti_{0.7}W_{0.3}O_2$ oxide than that on platinised Vulcan, the activity in hydrogen oxidation reaction decreased in comparison to commercial Pt/C [9].

Considering the mentioned facts, we decided to develop a novel support consisting of a composite of activated carbon and $Ti_{(1-x)}W_xO_2$ mixed oxide. The presence of the activated carbon makes the synthesis complicated, since earlier studies showed that it prefers the formation of segregated titania and tungsten-oxide phases, and the titania is presented in anatase phase that is disadvantageous for the incorporation of W [10].

Accordingly, we have developed a new multistep sol-gel synthesis method optimized for preparation of $Ti_{(1-x)}W_xO_2$ – activated carbon composites with almost exclusive tungsten incorporation into the rutile lattice. The optimization of the synthesis route, along with a structural and functional assessment of the synthesis products were described in a previous publication [10]. In the present work our aim is to give a more elaborate insight into the formation of the $Ti_{0.7}W_{0.3}O_2$-C composite material. To this end the influence of the heat treatment steps on the chemical states of the components is explored in a series of *in situ* XPS experiments, during which the inert gas annealing and the reduction were carried out in the preparation chamber of the photoelectron spectrometer, thus air exposure between the steps was avoided. The findings are analyzed in terms of structural development observed by XRD after each heat treatment step. Novel scanning electron microscopy data are shown to demonstrate the improved agglomeration resistance of the carbon-containing composite. Electrochemical data demonstrate the promising performance of the $Ti_{(1-x)}W_xO_2$ – activated carbon composite supported Pt electrocatalysts. The results are completed by the analysis of the electrochemical surface area values for the composite supported catalysts determined from hydrogen underpotential deposition (H-UPD) and CO stripping voltammetry.

2 Experimental

2.1 Synthesis of $50Ti_{0.7}W_{0.3}O_2$-50C materials

Detailed description of the synthesis procedure and its optimization can be found in [10]. Here the main features of the optimized process are briefly summarized (Fig. 1).

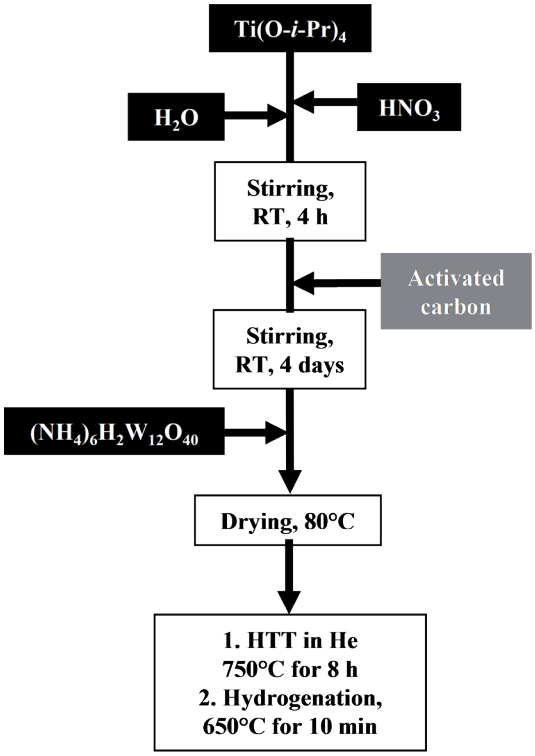

Fig. 1 Flow chart for preparing $50Ti_{0.7}W_{0.3}O_2$-50C composite materials by using sol-gel-based multistep synthesis

In order to prepare the composite support containing mixed oxide with Ti/W atomic ratio of 70/30 ($Ti_{0.7}W_{0.3}O_2$) and activated carbon in weight percent ratio 50:50 (denoted as $50Ti_{0.7}W_{0.3}O_2$- 50C), first transparent acidic TiO_2 colloidal solution was made by adding concentrated HNO_3 to a vigorously stirred mixture of titanium-isopropoxide and distilled water. Activated carbon (CABOT, Black Pearls 2000, S_{BET}= 1475 m^2 g^{-1}) was added after 4 h stirring at room temperature (RT). In order to facilitate the formation of rutile nuclei, the mixture was aged at RT for 0.5-4 days. After the aging, $(NH_4)_6H_2W_{12}O_{40}$ was added and the solvent was evaporated at 80 °C. The powder was dried at 80 °C overnight. The obtained powder has been submitted to a two-step high temperature treatment (HTT): after the drying procedure at 80°C the sample was treated in He at T= 750°C for 8 hours then reduced in hydrogen-water mixture (H_2:H_2O= 95:5 v/v ratio) at 650°C for 10 minutes and cooled down in helium to RT. Carbon-free $Ti_{0.7}W_{0.3}O_2$ was also prepared for reference purposes. The original reduction process of Ref. [8] (heating with stoichiometric amount of Zr foil at 750°C for up to 2 days) was replaced with the much faster two-step heat treatment described above.

The $Ti_{0.7}W_{0.3}O_2$-C composite material, the carbon-free $Ti_{0.7}W_{0.3}O_2$ and the pure activated carbon have been loaded with 40 wt% Pt via the $NaBH_4$-assisted ethylene-glycol (EG) reduction method [11]. The material was washed with water by centrifugation and dried at 80 °C overnight.

2.2 Physicochemical characterization

The powder X-ray diffraction (XRD) patterns were obtained in a Philips model PW 3710 based PW 1050 Bragg-Brentano parafocusing goniometer using CuK_α radiation (λ= 0.15418 nm), graphite monochromator and proportional counter. Silicon powder (NIST SRM 640) was used as an internal standard and the scans were evaluated with profile fitting methods. The cell parameters of the crystalline phases were determined from the fitted d-values. Crystallite sizes were calculated from reflection line broadening using the Scherrer-equation. Since isovalent tungsten incorporation into the rutile lattice causes a characteristic distortion (expansion along the *a*-axis and contraction along the *c*-axis of the unit cell, [4,9,12]), XRD is an excellent method for assessing the extent of modification.

Transmission Electron Microscopy (TEM) studies of the samples were made by use of a FEI Morgagni 268D type transmission electron microscope (accelerating voltage: 100 kV, W-filament). The fresh samples and those used in electrochemical stability tests were prepared by grinding and dispersing of the resulted powder in ethanol using an ultrasonic bath. After electrochemical experiments catalysts were removed from the electrodes with isopropanol in an ultrasonic bath. A volume of the obtained suspension was pipetted onto a carbon coated copper grid. The average diameter was calculated by measuring the diameters of at least 350 randomly selected metal particles from the non-aggregated areas in at least tree micrographs of each sample.

The response of the $50Ti_{0.7}W_{0.3}O_2$-50C composite material to the two-stage annealing was followed by *in situ* X-ray photoelectron spectroscopy (XPS) experiments. Data were taken with MgKα (1253.6 eV) radiation using an EA125 electron spectrometer manufactured by OMICRON Nanotechnology GmbH (Germany). Spectra were recorded in the Constant Analyser Energy mode of the energy analyser with 30 eV pass energy resulting in a spectral resolution of 1 eV.

The powder samples were sedimented on standard OMICRON sample plates from hexane suspension. Steps of the heat treatment were modeled by annealing the sol-gel synthetized material in Ar at 620 °C for 8 hours and reducing it in pure H_2 for 10 min at 500°C in the high pressure preparation chamber of the electron spectrometer. XPS spectra were taken in the as synthetized, Ar annealed and reduced state, without air exposure. The sensitivity of the final product for oxidation was assessed after a deliberate venting for 30 min. In order to facilitate data evaluation, reference spectra of WO_3 and WO_2 were also measured; in the latter case the surface oxide layer was removed by annealing in vacuum at 500°C.

Binding energies were referenced to the graphite component of the C 1s spectrum of the support (284.4 eV binding energy). Data were processed using the CasaXPS software package [13] by fitting the spectra with Gaussian-Lorentzian product peaks after removing a Shirley or linear background. Nominal surface compositions were calculated using the XPS MultiQuant software package [14-15], with the assumption of homogeneous depth distribution for all components. Chemical states were identified by XPS databases [16-17] and with the help of the related literature.

2.3 Electrochemical characterization

The 40 wt% Pt/$50Ti_{0.7}W_{0.3}O_2$-50C electrocatalysts were investigated by means of cyclic voltammetry and CO_{ad} stripping technique.

The working electrode was prepared by supporting the electrocatalysts on a glassy carbon electrode (d = 0.3 cm, geometric surface area A = 0.0707 cm^2). Before each test the glassy carbon disc was polished with 0.05 μm alumina to obtain a mirror finish, followed by ultrasonic cleaning in water (18.2 MΩ cm), isopropanol and again water to remove any traces of organic impurities. The samples under study were deposited onto the glassy carbon by means of a catalyst ink. 5 mg of the electrocatalyst, 0.5 ml of EG, 0.2 ml of isopropanol and 30 μl of Nafion solution (DuPont™ Nafion® PFSA Polymer Dispersions DE 520) were dispersed in an ultrasonic bath for 45 minutes, resulting in a homogeneous ink. After ultrasonic dispersion an 1.3 μl aliquot has been dropped over the glassy carbon surface and dried under an infrared lamp for 30 minutes leading to a homogeneous coating. Pt wire was used as counter electrode. The reference electrode was Ag/ AgCl electrode but all potentials are given on the reversible hydrogen electrode (RHE) scale. The applied electrolyte was 0.5 M H_2SO_4. Prior to the measurements, the electrode was activated by potential cycling 100 times in the range 0.05 and 1.25 V at a scan rate of 1000 mV s^{-1}. After the activation procedure, CO stripping measurements were done in 0.5 M H_2SO_4 in the potential range of 0.05-1.05 V at a scan rate of 10 mV s^{-1}. Gaseous CO was fed into the cell for 30 min while maintaining the electrode potential constant at 0.02 V. After CO removal from the solution (Ar purge for 30 min), the working electrode was subjected to a cyclic voltammetric (CV) measurement. For comparison PtRu/C, considered as the state-of-the art CO-tolerant electrocatalyst, (Quintech C-20/10-Pt/Ru, Pt=20wt%, Ru=10wt% on Vulcan; denoted hereafter as PtRu/C) was also studied in the CO_{ads} stripping after Ar purging. Upon the Q_{CO} charges calculation the current of the base line voltammogram was subtracted in the potential region of the CO oxidation peak.

The electrochemical stability was tested by potential cycling between 0.05 and 1.25 V at a scan rate of 50 mV s^{-1} for 5000 cycles. The measurements took 66.7 hours. The Q_{H-UPD} charges (where H-UPD means the hydrogen underpotential deposition) were calculated using conventional baseline correction.

Electrochemically active surface area was calculated from the charge required either to oxidize a pre-adsorbed monolayer of CO in a stripping ($ECSA_{CO}$, assuming 420 μC cm_{Pt}^{-2} (Eq. (1)) or to adsorb/desorb a layer of hydrogen in the so-called H_{UPD} region in a CV ($ECSA_{H-UPD}$, assuming 210 μC cm_{Pt}^{-2} (Eq. (2)) [18-19]:

$$\frac{A}{m} = \frac{\frac{Q_{CO}}{420\mu Ccm^{-2}}}{m} \quad (1)$$

$$\frac{A}{m} = \frac{\frac{Q_{H-UPD}}{210\mu Ccm^{-2}}}{m} \quad (2)$$

Relative errors were calculated as the standard deviation of at least three independent measurements. The potential errors during the measurements include inaccuracies of catalyst weighting, inhomogeneities of the catalyst suspensions and correction of double layer currents. The protocol of the electrochemical measurements was previously tested on commercially available standard 40 wt% Pt/C electrocatalyst (QuinTech, C-40-Pt) with respect to the specifications from the manufacturer.

3 Results and discussion

According to XRD phase analysis results presented in Fig. 2 the duration of the RT aging of the Ti-sol in the presence of carbon strongly determines the size and crystal structure of the $Ti_{0.7}W_{0.3}O_2$-C composites obtained after addition of the W precursor. As shown in Fig. 2 the time of aging was varied between 12 h and 4 days. Upon the increase of the aging time the rutile/anatase (R/A) ratio increased significantly both before (Fig. 2A) and after high temperature treatment (HTT) in He and reduction in H_2 (Fig. 2B). As demonstrated in Fig. 2A and 2B at least 2 days of aging is necessary to avoid the presence of anatase TiO_2 (JCPDS card 21-1272). Upon increasing the time of aging from 12 h to 4 days (Fig. 2B) the relative abundance of non-incorporated monoclinic crystalline WO_2 phase (JCPDS card 86-0134) decreased from 38 % to 8 %. When the aging procedure was short (0.5-1 day) a trace amount (~2 %) of unreduced monoclinic WO_3 oxide phase (JCPDS card 72-0677) was also observed (Fig. 2B).

In case of the sample aged for 4 days and treated in He at 750°C for 8 h and H_2 at 650°C for 10 min (Fig. 2B), almost pure (R/WO_2= 92/8) rutile TiO_2 phase (JCPDS card 21-1276) can be achieved. The results clearly show that the presence of rutile phase TiO_2 particles before the two-step heat treatment is prerequisite for efficient tungsten incorporation.

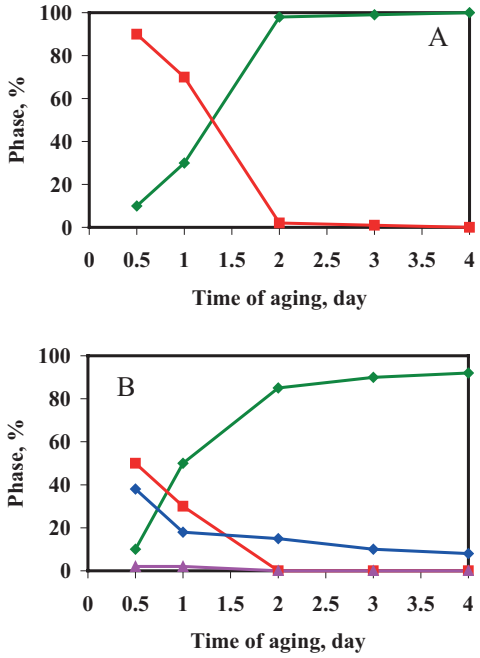

Fig. 2 The effect of the aging time of the Ti-sol on the structure of $Ti_{0.7}W_{0.3}O_2$-C composites. XRD measurements before (A) and after HTT and reduction (B). ◆ – rutile, ■– anatase, ▲ – WO_3, ◆ – WO_2.

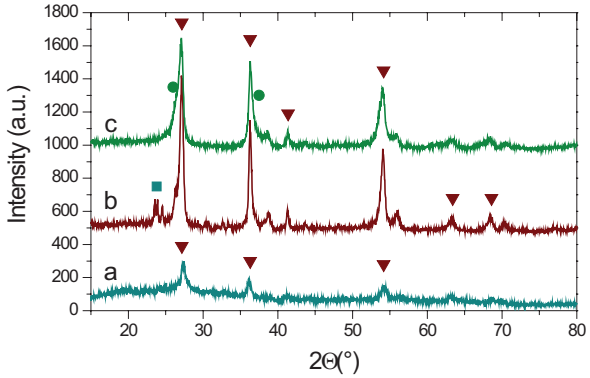

Fig. 3 XRD patterns of $Ti_{0.7}W_{0.3}O_2$-C composites before HTT in He (A), after HTT (B) and after reduction (C). ▼ – rutile, ■ – WO_3, ● – WO_2.

In Ref. [10] structural changes of the sol-gel synthetized material as the result of the two-step heat treatment (inert gas annealing and subsequent reduction) were discussed in connection with details of the synthesis process. In the present work we would like to get a deeper insight into the role of the annealing steps, thus Fig. 3 compares the influence of the inert gas annealing and the reduction on the XRD patterns of the $Ti_{0.7}W_{0.3}O_2$-C composite material.

The powder obtained before any HTT resulted in rutile crystallites (Fig. 3, sample **a**). After the heat treatment in He at 750°C for 8 h (sample **b**), besides the presence of rutile phase, small amount of non-incorporated tungsten in the form of segregated WO_2 and WO_3 phases was also observed ($R/WO_3/WO_2$= 93/5/2). The changes in the lattice parameters (a= 4.660 Å, c= 2.925 Å, while pure rutile TiO_2 structure has a= 4.593 Å, c= 2.959 Å) confirms the presence of tungsten

Table 1 Summary of the XPS analysis of the 50% $Ti_{(1-x)}W_xO_2$ - 50% C sample before annealing, after the high temperature annealing in inert gas, after reduction and after air exposure. Reference data for WO_3 and WO_2 are also included.

50% $Ti_{(1-x)}W_xO_2$ - 50% C							
Treatment	Peak binding energy (eV), assignment, relative contribution			Composition (atomic %)			
	W $4f_{7/2}$	Ti $2p_{3/2}$	O 1s	W	Ti	O	C
Without treatment	35.9 W^{6+} (49%)	459.2 Ti^{4+} (TiO_2)	530.8 (WO_x, TiO_x)	2.2	2.8	19.3	75.7
	35.0 W^{5+} (51%)		532.7 (-OH, CO_x)				
			534.3 (water)				
Annealing in Ar at 620°C for 8 h	35.9 W^{6+} (34%)	459.1 Ti^{4+} (96%)	530.8 (WO_x, TiO_x)	2.6	2.5	14.1	80.9
	34.9 W^{5+} (23%)	457.2 Ti^{3+} (4%)	532.8 (-OH, small)				
	33.7 W^{4+} (42%)						
Reduction in H_2	35.9 W^{6+} (4%)	459.2 Ti^{4+} (95%)	530.8 (W, TiO_x)	2.3	2.4	14.0	81.3
	33.5 W^{4+} (63%)	457.0 Ti^{3+} (5%)	532.8 (-OH, small)				
	32.5 W^{2+} (21%)						
	31.5 W^0 (12%)						
Air exposure	35.6 W^{6+} (39%)	459.0 Ti^{4+} (100%)	530.6 (WO_x, TiO_x)	2.4	2.4	15.4	79.8
	34.8 W^{5+} (15%)		532.6 (-OH, small)				
	33.5 W^{4+} (41%)						
	32.6 W^{2+} (5%)						
WO_3 reference							
Without treatment	35.9 W^{6+} (100%)	n.a.	531.0 (WO_x)	26.0	n.a.	74.0	n.a.
WO_2 reference							
Annealing in vacuum at 500°C	32.8 W^{4+} (100%)	n.a.	530.9 (WO_x)	36.0	n.a.	64.0	n.a.

incorporated into the unit cell (W_{subst}= 25 %). After reduction in H_2 (sample **c**) almost pure rutile phase was obtained (R/WO_2= 92/8) with high level of crystallinity (98-100 %) and high degree of W incorporation (W_{subst}= 30 %). After the reduction in H_2 further minor changes were observed in the lattice parameters (*a*= 4.670 Å, *c*= 2.920 Å).

In a series of experiments the effects of the two-step heat treatment on the composition of the $Ti_{(1-x)}W_xO_2$ – activated carbon composite and the chemical state of the metal constituents were assessed by XPS measurements. The heat treatments were carried out in the high pressure chamber of the electron spectrometer, thus no air exposure was encountered between the treatment steps. Fig. 4 summarizes the W 4f core level spectra obtained at the stages of this *in situ* study.

During analysis of spectra, the contribution of the Ti 3p band around 37.6 eV was subtracted. The peak shapes, binding energies and assignments of the W 4f chemical states were taken from the literature [20-25] and confirmed by reference spectra of pure WO_3 (W^{6+}) and WO_2 (W^{4+}). In particular, W^{4+} states are characterized by a compound peak shape consisting of spin-orbit doublets of a main peak and a satellite, as a result of co-existence of two fundamentally differently screened final states.

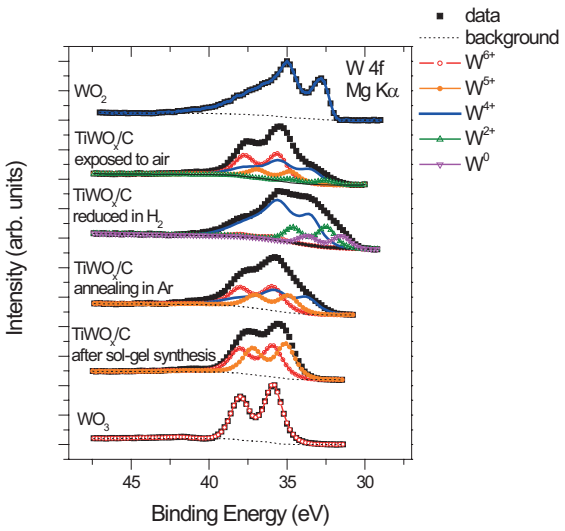

Fig. 4 W 4f core level spectra of the 50$Ti_{(1-x)}W_xO_2$-50C composite after the sol-gel synthesis, after the high temperature annealing in inert gas, after reduction and after air exposure. Reference spectra of WO_3 and vacuum annealed WO_2 are also included.

After sol-gel synthesis and drying XRD indicates the presence of structurally imperfect rutile crystallites. XPS also reveals Ti^{4+} ionic states (see Table 1), while the W 4f spectrum can be described by two spin-orbit doublets with

$4f_{7/2}$ components around 35.9 eV (W^{6+}) and 35.0 eV, which is only slightly above the values reported to W^{5+}. Literature data indicate that tungsten bronzes show this two-component W 4f spectrum; in particular, H_xWO_3-like materials have very similar W 4f spectra to that measured in this system [26-27]. Therefore it is plausible that the starting material for the present catalyst after drying is some hydrogenated tungsten oxide along with TiO_2. The presence of hydrogenated species is suggested by also the O 1s signals, where the major contribution at 530.8 eV (tungsten oxides, probably along with Ti-oxides) is accompanied by a band around 532.7 eV, which is most probably due to –OH species, while a tiny amount of adsorbed water is suggested by an O 1s contribution at an even higher binding energy. Lack of any N 1s emission precludes ammonium tungsten bronze formation during the synthesis.

In the XRD experiment the lengthy annealing in inert gas significantly improved the crystalline quality of the rutile TiO_2. Although the *in situ* treatment in the electron spectrometer was performed at somewhat lower temperature (620°C) in Ar, notable changes were seen in the tungsten chemical states. The modeling of the complex W 4f line shape required at least 3 spin-orbit doublets. The first two, the 35.9 eV (W^{6+}) and 34.9 eV (W^{5+}) ones were already present in the as received state, although the hydrogenation level of the system certainly decreased, thus the W^{5+} component now should rather be related to tungsten in connection with oxygen vacancy sites. The third component, with a compound peak shape located around 33.7 eV, can be assigned to W^{4+} states. It may be worth to note that its binding energy is somewhat higher than that of W^{4+} in WO_2 (32.8 eV), which may be indicative of a different chemical environment for the tungsten cations. A similar shift is seen in the Ti $2p_{3/2}$ binding energy (from 458.8 eV in pure TiO_2 to 459.3 eV), as also mentioned in the literature [28]. A weak new component around 457 eV suggests that a slight reduction of TiO_2 also took place. The O 1s contribution arising from -OH species became weak giving a slight asymmetric tail at the high binding energy side of the metal-oxide related main peak.

These data suggest that the transformation of the material towards the mixed oxide state starts already during the high temperature heat treatment. Indeed, it has been proposed that rutile, which has the same crystal structure and metal-O bond length as WO_2, can facilitate and stabilize the W^{4+} ions, immediately accommodating the formed WO_2 species [29]. Reduction of WO_3 to WO_2 in WO_x/TiO_2 catalysts and relative stability of W^{4+} species on the TiO_2 surface has been also demonstrated in Refs. [30-31].

Nevertheless, XRD data reveal that complete tungsten incorporation and activation cannot be achieved without the reduction step. In the *in situ* XPS study the 10 minute reduction was performed at a relatively low temperature (500°C) in pure H_2.

While the other components of the system show only very small changes upon reduction, the W 4f spectrum again indicates significant chemical state modifications. The signals of the higher oxidation states become negligible; modeling of the spectrum can be achieved by the previously mentioned complex W^{4+} line shape, along with two additional doublets: a peak pair around 32.5 eV, which is due to W^{2+} and a low binding energy doublet at 31.5 eV, which indicates the presence of zero-valence tungsten. This latter may arise from metallic tungsten or tungsten carbide, which can form as a result of a reaction between metallic tungsten and the graphite support. The data show that reduction of tungsten in the presence of hydrogen at elevated temperatures is a very easy process and proceeds readily until the metallic state. As in the presence of water vapour the unwanted reduction of WO_2 to metallic W becomes hindered, [32], adding a small amount of water to the H_2 gas turns out to be advisable [32].

The most drastic effect expected during reduction is the formation of metallic deposits from non-incorporated tungsten; it was indeed detected in the *in situ* XPS experiment, in spite of the lower reduction temperature. On the other hand, XRD data revealed the presence of WO_2 without any metallic phase after the reduction in the moist hydrogen. As metallic W oxidizes into WO_3 upon air exposure [24], the WO_2 content may have formed as a result of water-induced stopping of the reduction of non-incorporated tungsten at the 4+ oxidation state.

After the *in situ* heat treatment/reduction procedure, the sample was exposed to air for two days, from which the stability of the material against oxidation can be judged. Indeed, using the fitting components identified in the previous treatments, it turns out that a significant W^{6+} component accompanied by some W^{5+} developed during the air exposure, while the highly reduced tungsten species (metallic and W^{2+}) almost completely disappeared.

This observation is in accordance with literature results showing that both W and WC are readily oxidized towards W^{6+} upon room temperature air exposure [24]. The estimated amount of W^{4+} also considerably decreased.

It is reasonable to assume that incorporation of tungsten into the rutile lattice provides some protection against both excessive reduction and oxidation, while non-incorporated W is more easily changes its oxidation state. Therefore, the W^{4+} signal remaining after air exposure can be at least partly associated with tungsten in the mixed oxide phase.

Quantitative evaluation of the XPS data indicate that the carbon content is around 51-52 mass%, which is in excellent agreement with the planned value. Nevertheless, the tungsten content is somewhat high (see Table 1), probably above the solubility limit, which explains why non-incorporated W was evidenced in the composite material.

Figures 5A and 5B show SEM images of $50Ti_{0.7}W_{0.3}O_2$- 50C composite before and after deposition of 40 wt% Pt, respectively. SEM image of the $Pt/Ti_{0.7}W_{0.3}O_2$ electrocatalyst (Fig. 5C) was given for comparison. In our recent study it has

Table 2 Compositional data on $50Ti_{0.7}W_{0.3}O_2$-50C composite (sample 1) and $Pt/50Ti_{0.7}W_{0.3}O_2$-50C electrocatalysts (sample 1-Pt)

Samples	Ti/W (at/at)			(Ti+W+O)/C (wt/wt)		Pt (wt%)	
	EDS	XRF	XPS	EDS	XPS	EDS	XRF
1	69.3/30.7	69.1/30.9	49.0/51.0	53.2/46.8	48.3/51.7	-	-
1-Pt	72.3/27.7	73.0/27.0	71.4/28.6	51.0/49.0	41.5/58.5	38.6	41.8

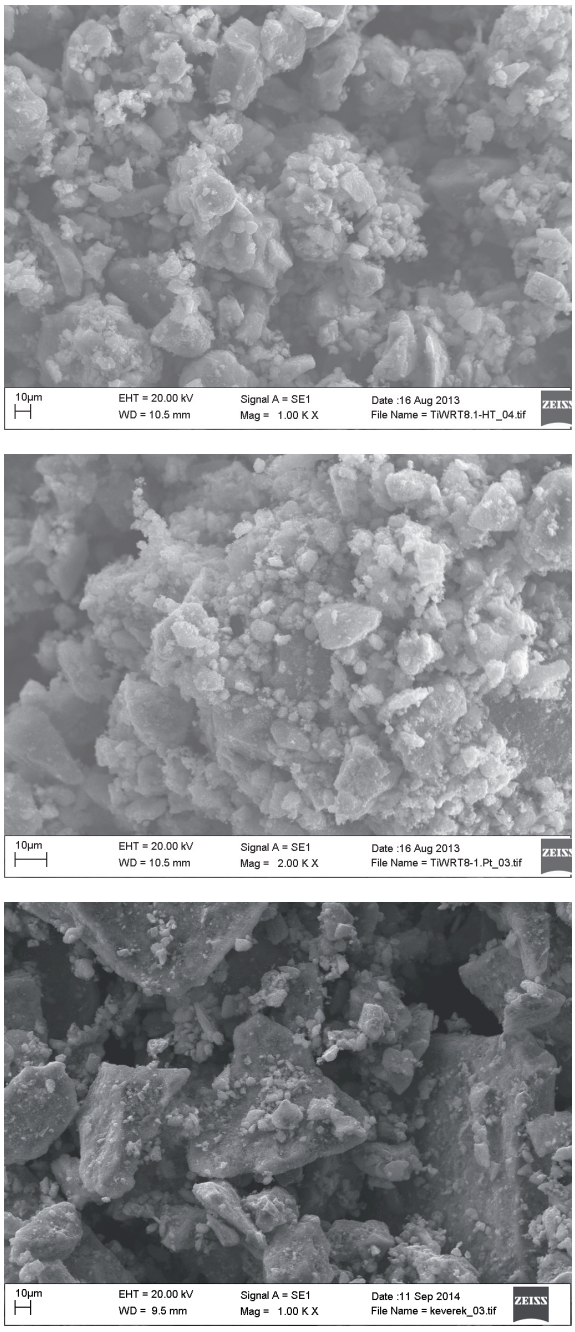

Fig. 5 SEM images of $50Ti_{0.7}W_{0.3}O_2$-50C composite (A) and $Pt/50Ti_{0.7}W_{0.3}O_2$-50C (B), $Pt/Ti_{0.7}W_{0.3}O_2$ (C) electrocatalysts.

been demonstrated [10] that after HTT in He at 750°C for 8 hours the BET surface area of $50Ti_{0.7}W_{0.3}O_2$-50C sample was about SBET= 640 m^2 g^{-1}. This observation is substantiated by the evidence from Fig. 5, namely that in the presence of activated carbon the dispersion of the mixed oxide particles is considerably higher. High value of the BET surface area obtained after HTT demonstrates that in the presence of activated carbon the particles of the composite materials are successfully protected from sintering.

The results of SEM-EDX measurements showed that the atomic composition of the samples and the individual particles was highly homogenous. Table 2 summarizes the results of the EDS, XRF and XPS measurements on the $50Ti_{0.7}W_{0.3}O_2$-50C composite and the $Pt/50Ti_{0.7}W_{0.3}O_2$-50C electrocatalyst. The Ti/W atomic ratios and the measured $Ti_{0.7}W_{0.3}O_2$/C= 50:50 weight ratios are in good agreement with the expected one. Results demonstrate that the Ti/W ratio of the $Ti_{(1-x)}W_xO_2$ mixed oxide can be controlled by varying the amount of the Ti and W precursors, respectively. As was mentioned above, significant difference could be seen only in case of the XPS results. The increased ratio of W (from 30 to 51%) can be explained by the partial segregation of the non-incorporated W-oxide species to the surface of the mixed oxide grains. The decrease of the relative tungsten content seen by XPS after Pt deposition is presumably the combined consequence of (i) shadowing of the segregated tungsten species by the Pt particles or (ii) some dissolution of the segregated tungsten oxides during Pt deposition. EDS analysis of different regions of the electrocatalyst revealed the uniform distribution of the Pt nanoparticles on $Ti_{0.7}W_{0.3}O_2$-C composite materials with an average Pt content of 38.6 wt%, this value is in an agreement with the planned 40 wt%.

Figure 6 depicts TEM micrograph of the Pt supported on $Ti_{0.7}W_{0.3}O_2$ mixed oxide along with the corresponding histogram for particle size distribution. TEM image in Fig. 6 reveals that some of the small Pt particles are separated while others are included in raspberry-like agglomerates. The mean diameter derived from the size distribution is 7.28 ± 3.49 nm. The agglomeration may be due to difficulties observed upon deposition of Pt by the $NaBH_4$-assisted EG reduction method on pure $Ti_{0.7}W_{0.3}O_2$ mixed oxide. Our results demonstrate that this method was quite ineffective in case of oxide supports, but can be successfully used for the preparation of carbon and $Ti_{0.7}W_{0.3}O_2$-C supported Pt catalysts.

The uniform distribution of spherical Pt particles with mean diameter of 2.3 ± 0.8 nm and 4.5 ± 1.8 nm was verified via TEM imaging for the $Pt/Ti_{0.7}W_{0.3}O_2$-C (Fig. 7A) and Pt/C (Fig. 7B) electrocatalysts, respectively. Certain increase of the Pt particle size after electrochemical stability test experiments was demonstrated (see Fig. 7C-D; note the difference in the

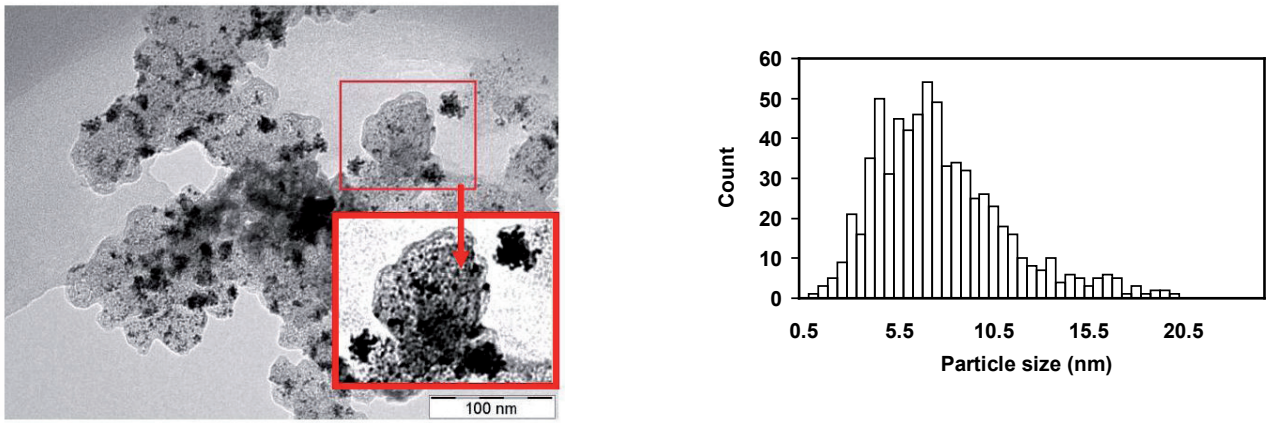

Fig. 6 TEM image and histogram of particle size distribution of the $Pt/Ti_{0.7}W_{0.3}O_2$ electrocatalyst.

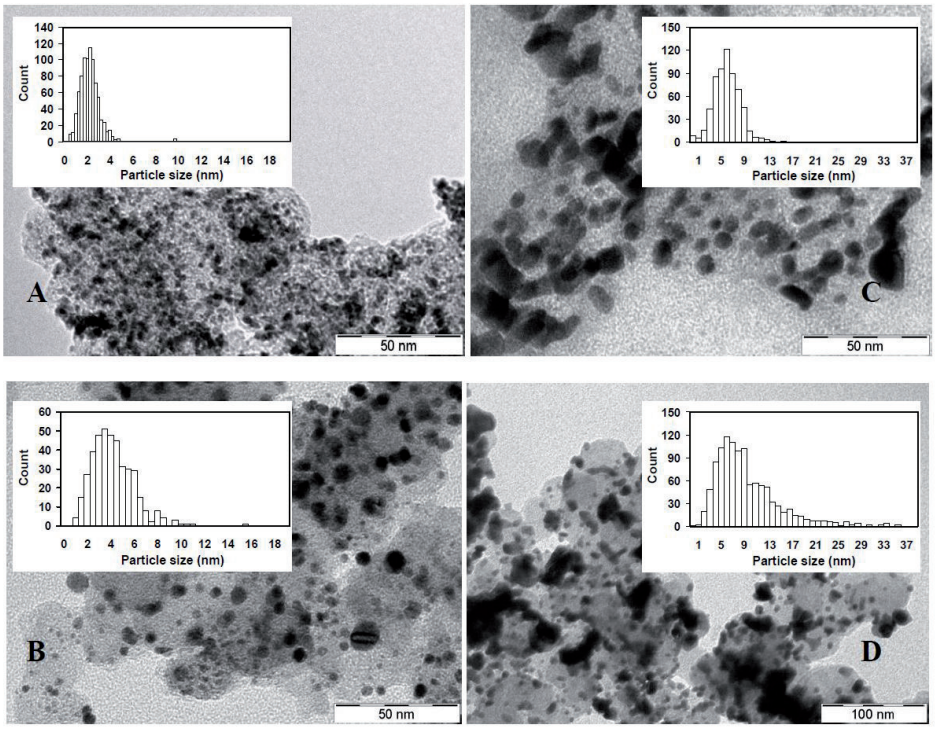

Fig. 7 TEM images and histogram of particle size distribution before (left) and after the electrochemical stability test experiments (right) for $Pt/Ti_{0.7}W_{0.3}O_2$-C (A, C) and Pt/C (B, D) catalysts.

magnification). After 5000 cycles, some extent of sintering and agglomeration of the Pt nanoparticles was observed for both catalysts. The increase of the Pt particle size to 6.5 ± 2.3 nm and 10.0 ± 5.7 nm was observed on the $Pt/Ti_{0.7}W_{0.3}O_2$-C and the Pt/C catalysts, respectively. These results confirm that upon using of the composite support, more effective protection of Pt nanoparticles from agglomeration can be reached.

Figure 8A compares the Ar-purged CO-stripping curves recorded on the $Pt/Ti_{0.7}W_{0.3}O_2$-C sample with those obtained on the $Pt/Ti_{0.7}W_{0.3}O_2$ electrocatalyst. For comparison our results obtained on unmodified parent Pt/C and PtRu/C (Quintech) with Pt = 20 wt%, considered as the state-of-the art CO-tolerant electrocatalyst, were also included (see Fig. 8B). During the first cycle after CO admission on both catalysts supported on the composite material and $Ti_{0.7}W_{0.3}O_2$ mixed oxide a "pre-peak" located between ~200 and ~550 mV was observed (Fig. 8A). It is necessary to mention that the appearance of the "pre-peak" on the Ar-purged CO_{ads} stripping voltammograms obtained on both catalysts resemble those commonly observed in the literature for CO tolerant W-modified Pt catalysts [5-6,33].

On the $Ti_{0.7}W_{0.3}O_2$-C composite supported Pt catalyst the "pre-peak" was followed by a narrow peak at 710 mV. On the Pt/C sample (see Fig. 8B) the main CO_{ads} stripping peak is located at ca. 820 mV. The position of this peak is shifted towards positive potentials by 110 mV with respect to the main peak observed on the $Pt/Ti_{0.7}W_{0.3}O_2$-C catalyst, thus demonstrating an enhanced tolerance to CO for the composite supported catalyst. Similar increased activity to CO_{ads} electrooxidation reaction was demonstrated for CO tolerant Pt/WO_x and $Pt\text{-}WO_x/C$ catalysts [5,6,33]. Moreover

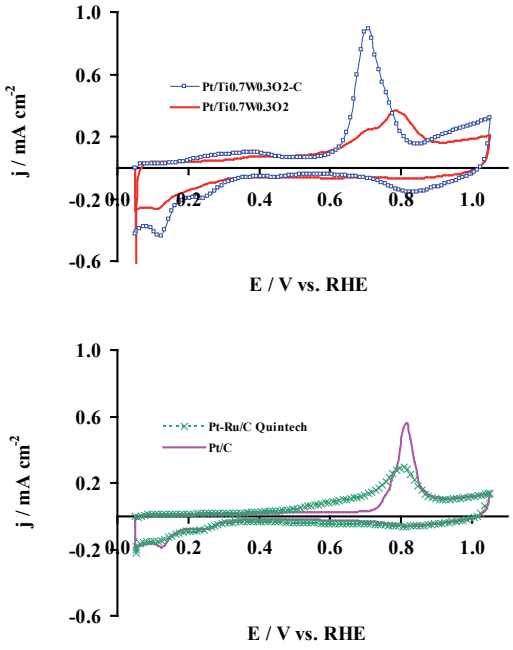

Fig. 8 CO_{ads} stripping voltammogram after Ar purging on $Pt/Ti_{0.7}W_{0.3}O_2$-C, $Pt/Ti_{0.7}W_{0.3}O_2$ (with 20 wt% C added) (A) and Pt/C, PtRu/C catalysts (B). Recorded in 0.5 M H_2SO_4 at 10 mV·s^{-1}, T= 25 °C.

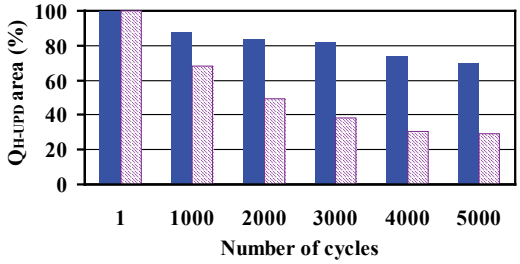

Fig. 9 Comparison of the integrated Coulombic charge (Q_{H-UPD}) loss of $Pt/Ti_{0.7}W_{0.3}O_2$-C (■) and Pt/C (▨) catalysts as a function of the number of cycles. Recorded in 0.5 M H_2SO_4 by potential cycling between 0.05 and 1.25 V at 50 mV·s^{-1}, T= 25 °C. The measurements took 66.7 hours. The Q_{H-UPD} charges, associated with hydrogen adsorption/desorption, were calculated using conventional baseline correction.

for $Pt/Ti_{0.7}W_{0.3}O_2$ electrocatalysts it has been proposed [8] that not only the presence of W but also TiO_2 contributes to the higher activity for CO oxidation.

The CO_{ads} stripping voltammogram on $Pt/Ti_{0.7}W_{0.3}O_2$ (see Fig. 8A) shows two CO_{ads} electrooxidation peaks at 710 and 780 mV. According to literature data not only the size but even the nanostructure of the platinum has detrimental effect on the onset potential of CO oxidation [34]. The presence of two electrooxidation peaks was ascribed by Maillard et al. [35-36] to the CO oxidation on Pt nanoparticles with different crystallographic orientations and/or different structures (for example, due to the agglomeration of Pt nanoparticles and formation of nano-grained structures with high surface defect density (steps, intergrain boundaries)). As shown in Fig. 6 the $Pt/Ti_{0.7}W_{0.3}O_2$ sample contains large amount of highly agglomerated raspberry-like particles in a quite broad particle size distribution. Multiple peaks in CO stripping voltammogramm may be ascribed to the inhomogeneity of the particle sizes in this sample.

The ECSA values can be calculated from the charge associated with a CO monolayer adsorbed onto the Pt nanoparticles ($ECSA_{CO}$) and from hydrogen adsorption/desorption region ($ECSA_{H-UPD}$) observed on the cyclic voltammogramms (CVs, not shown). In Ref. [10] data from CO stripping were published; in this work $ECSA_{H-UPD}$ was also determined and the two values were compared.

It is necessary to mention that a challenge for the surface area determination by both methods is the appropriate choice of the integration limits and the subtraction of background currents [18-19]. In accordance with literature data [33,35] the increased values of Q_{H-UPD} obtained for Pt/WO_x electrocatalysts can be correlated with the formation of tungsten bronzes H_xWO_3 or that of substoichiometric tungsten oxides WO_{3-x}. The formation of tungsten bronzes is catalyzed by the presence of Pt because adsorbed H spills over from the Pt sites to the WO_x support. In the case of WO_x-modified Pt catalysts both methods of the ECSA calculation have some uncertainties: (i) the formation of tungsten bronzes H_xWO_3 (if occurs) can influence the Q_{H-UPD} values; (ii) the "pre-peak" can not be separated well from the main CO oxidation peak (measured between 0.60-0.85 V) and the area of the "pre-peak" can not be calculated precisely, therefore the contribution of the "pre-peak" to the Q_{CO} was not taken into account. The corresponding ECSA values calculated for the $Pt/Ti_{0.7}W_{0.3}O_2$-C and the $Pt/Ti_{0.7}W_{0.3}O_2$ samples were $ECSA_{CO}= 33.4 \pm 4.4$ m^2/g_{Pt} ($ECSA_{H-UPD}= 47.3 \pm 3.5$ m^2/g_{Pt}) and $ECSA_{CO}= 13.8 \pm 1.8$ m^2/g_{Pt} ($ECSA_{H-UPD}= 16.6 \pm 1.4$ m^2/g_{Pt}), respectively.

A WO_2 crystallite phase not incorporated into the TiO_2-rutile lattice can be involved in the formation of tungsten bronzes H_xWO_3. Based on the XRD result, total incorporation of W was observed for carbon-free $Ti_{0.7}W_{0.3}O_2$ mixed oxide. Almost pure rutile phase (R/A= 92/8) with lattice parameters of $Ti_{0.7}W_{0.3}O_2$ (a=4.695, c= 2.910) and high crystallinity (98%) were obtained. On the contrary, in the $Ti_{0.7}W_{0.3}O_2$-C composite non-incorporated WO_2 (R/WO_2= 92/8) exists in addition to the rutile phase. The surface of these WO_2 crystallites easily oxidizes to WO_3 under oxidative conditions, which can incorporate hydrogen obtained by spillover from Pt particles. The difference observed between $ECSA_{H-UPD}$ and $ECSA_{CO}$ values for the $Pt/Ti_{0.7}W_{0.3}O_2$-C catalyst can thus be related to the formation of tungsten bronzes.

In spite of many uncertainties in the calculation of the ECSA values our results demonstrate that the surface area of the Pt catalyst supported on $Ti_{0.7}W_{0.3}O_2$-C composite materials is considerably larger than that of the $Pt/Ti_{0.7}W_{0.3}O_2$ sample. The observation is in agreement with the more dispersed nature of Pt on the composite substrate, as already revealed by the SEM and TEM results demonstrated above.

On the PtRu/C bimetallic catalyst (Fig. 8B) the CO_{ads} is oxidized over a broad potential region starting at potentials of ca. 350-400 mV with current maximum at 810 mV. It is necessary to mention that the maximum of the main peak observed in this work was shifted to higher potential comparing to the values usually accepted in the literature (650-700 mV [6,8]).

A major issue concerning the catalyst support durability is carbon corrosion, which occurs at potentials that are higher than 0.9 V vs. RHE [3]. Electrochemical corrosion of the carbon support causes the agglomeration and sintering of the Pt catalyst particles, which results in decreased activity of the catalysts [1-2].

Electrochemical stability of the Pt catalyst supported on the $Ti_{0.7}W_{0.3}O_2$-C composite and the home made Pt/C catalyst during 5000 cycles was compared (Fig. 9). As shown in Fig. 9, after 5000 cycles, the loss in the Q_{H-UPD} associated with hydrogen adsorption/ desorption was ca. 30 % and above 70 % for Pt/$Ti_{0.7}W_{0.3}O_2$-C and Pt/C catalysts, respectively. The more pronounced loss of activity in the Pt/C catalyst can be ascribed to the higher extent of sintering and agglomeration of the Pt nanoparticles during the 5000 cycles (Fig. 7C and 7D) compared to that observed for the $Ti_{0.7}W_{0.3}O_2$-C composite supported system.

4 Conclusion

Novel Pt electrocatalysts for fuel cell applications were prepared by introducing the $Ti_{0.7}W_{0.3}O_2$-C composite material as support.

$Ti_{0.7}W_{0.3}O_2$-C composite structure with high level of isovalent W incorporation was obtained by the proper tuning of the synthesis parameters. It is prerequisite for this to achieve pure rutile phase already at room temperature. SEM experiments revealed the more porous nature of the composite support material when compared to that of the carbon-free mixed oxide. Platinum deposited by the $NaBH_4$-assisted ethylene-glycol reduction method remained more disperse and stable on the composite than either on the carbon-free mixed oxide or on pure activated carbon.

These structural properties translated into enhanced electrocatalytic performance in terms of CO tolerance and long term stability when compared to traditional Pt/C or state-of-art CO tolerant PtRu/C catalysts.

Acknowledgement

The authors are grateful to the Hungarian Scientific Research Fund (OTKA, Grant №: K100793 and K77720) and the National Development Agency (Grant №: KTIA_AIK_12-1-2012-0014) for financial support.

References

[1] Meier, J. C., Galeano, C., Katsounaros, I., Topalov, A. A., Kostka, A., Schuüth, F., Mayrhofer, K. J. J. "Degradation Mechanisms of Pt/C Fuel Cell Catalysts under Simulated Start-Stop Conditions." *ACS Catalysis.* 2 (5). pp. 832-843. 2012. DOI: 10.1021/cs300024h

[2] Huang, S. Y., Ganesan, P., Popov, B. N. "Development of a Titanium Dioxide-Supported Platinum Catalyst with Ultrahigh Stability for Polymer Electrolyte Membrane Fuel Cell Applications." *Journal of American Chemical Society.* 131 (39). pp. 13898-13899. 2009. DOI: 10.1021/ja904810h

[3] Huang, S. Y., Ganesan, P., Popov, B. N. "Titania supported platinum catalyst with high electrocatalytic activity and stability for polymer electrolyte membrane fuel cell." *Applied Catalysis B: Environmental.* 102 (1-2). pp. 71-77. 2011. DOI: 10.1016/j.apcatb.2010.11.026

[4] Aryanpour, M., Hoffmann, R., DiSalvo, F. J. "Tungsten-Doped Titanium Dioxide in the Rutile Structure: Theoretical Considerations." *Chemistry of Materials.* 21 (8). pp. 1627-1635. 2009. DOI: 10.1021/cm900329k

[5] Pereira, L. G. S., dos Santos, F. R., Pereira, M. E., Paganin, V. A., Ticianelli, E. A. "CO tolerance effects of tungsten-based PEMFC anodes." *Electrochimica Acta.* 51 (19). pp. 4061-4066. 2006. DOI: 10.1016/j.electacta.2005.11.025

[6] Micoud, F., Maillard, F., Gourgaud, A., Chatenet, M. "Unique CO-tolerance of Pt-WO_x materials." *Electrochemistry Communications.* 11 (3). pp. 651–654. 2009. DOI: 10.1016/j.elecom.2009.01.007

[7] Tseung, A. C. C., Chen, K. Y. "Hydrogen spill-over effect on Pt/WO_3 anode catalysts." *Catalysis Today.* 38 (4). pp. 439-443. 1997. DOI: 10.1016/s0920-5861(97)00053-9

[8] Wang, D., Subban, C. V., Wang, H., Rus, E., DiSalvo, F. J., Abruña, H. D. "Highly Stable and CO-Tolerant Pt/$Ti_{0.7}W_{0.3}O_2$ Electrocatalyst for Proton-Exchange Membrane Fuel Cells." *Journal of American Chemical Society.* 132 (30). pp. 10218-10220. 2010. DOI: 10.1021/ja102931d

[9] Subban, C. V., Zhou, Q., Hu, A., Moylan, T. E., Wagner, F. T., DiSalvo, F. J. "Sol-Gel Synthesis, Electrochemical Characterization, and Stability Testing of $Ti_{0.7}W_{0.3}O_2$ Nanoparticles for Catalyst Support Applications in Proton-Exchange Membrane Fuel Cells." *Journal of American Chemical Society.* 132 (49). pp. 17531-17536. 2010. DOI: 10.1021/ja1074163

[10] Gubán, D., Borbáth, I., Pászti, Z., Sajó, I., Drotár, E., Hegedűs, M., Tompos, A. "Preparation and characterization of novel $Ti_{0.7}W_{0.3}O_2$-C composite materials for Pt-based anode electrocatalysts with enhanced CO tolerance." *Applied Catalysis B: Environmental.* 174. pp. 455-470. 2015. DOI: 10.1016/j.apcatb.2015.03.031

[11] Kim, P., Joo, J. B., Kim, W., Kim, J., Song, I. K., Yi, J. "$NaBH_4$-assisted ethylene glycol reduction for preparation of carbon-supported Pt catalyst for methanol electro-oxidation." *Journal of Power Sources.* 160 (2). pp. 987-990. 2006. DOI: 10.1016/j.jpowsour.2006.02.050

[12] Peters, E., Müller-Buschbaum, H. "Ueber ein niedervalentes Titan-Wolframoxid: $Ti_{0,54}W_{0,46}O_2$." (On a Low Valent Titanium Tungsten Oxide: $Ti_{0,54}W_{0,46}O_2$.) *Zeitschrift fuer Naturforschung B.* 51 (1). pp. 29-31. 1996. DOI: 10.1515/znb-1996-0107 (in German)

[13] Fairley, N. "CasaXPS: Spectrum Processing Software for XPS, AES and SIMS." Version 2.3.13. Casa Software Ltd, Cheshire. 2006. URL: http://www.casaxps.com

[14] Mohai, M. "XPS MultiQuant: Multimodel XPS Quantification Software." *Surface and Interface Analysis.* 36 (8). pp. 828-832. 2004. DOI: 10.1002/sia.1775

[15] Mohai, M. "XPS MultiQuant: Multi-model X-ray photoelectron spectroscopy quantification program." Version 3.00.16. 2003. URL: http://www.chemres.hu/aki/XMQpages/XMQhome.htm

[16] Wagner, C. D., Naumkin, A. V., Kraut-Vass, A., Allison, J. W., Powell, C. J., Rumble, J. R. Jr. "NIST X-ray Photoelectron Spectroscopy Database." Version 3.4, National Institute of Standards and Technology, Gaithersburg, MD. 2003. URL: http://srdata.nist.gov/xps/

[17] Moulder, J. F., Stickle, W. F., Sobol, P. E., Bomben, K. D. "*Handbook of X-ray Photoelectron Spectroscopy.*" Perkin-Elmer Corp., Eden Prairie, Minnesota. 1992.

[18] Schulenburg, H., Durst, J., Müller, E., Wokaun, A., Scherer, G. G. "Real surface area measurements of Pt_3Co/C catalysts." *Journal of Electroanalytical Chemistry.* 642 (1). pp. 52-60. 2010. DOI: 10.1016/j.jelechem.2010.02.005

[19] Mayrhofer, K. J. J., Strmcnik, D., Blizanac, B. B., Stamenkovic, V., Arenz, M., Markovic, N. M. "Measurement of oxygen reduction activities via the rotating disc electrode method: From Pt model surfaces to carbon-supported high surface area catalysts." *Electrochimica Acta.* 53 (7). pp. 3181-3188. 2008. DOI: 10.1016/j.electacta.2007.11.057

[20] Colton, R. J., Rabalais, J. W. "Electronic-structure of tungsten and some of its borides, carbides, nitrides, and oxides by X-ray electron-spectroscopy." *Inorganic Chemistry.* 15 (1). pp. 236-238. 1976. DOI: 10.1021/ic50155a049

[21] Masek, K., Libra, J., Skála, T., Cabala, M., Matolín, V., Cháb, V., Prince, K.C. "SRPES investigation of tungsten oxide in different oxidation states." *Surface Science.* 600 (8). pp. 1624-1627. 2006. DOI: 10.1016/j.susc.2005.11.048

[22] Xie, F. Y., Gong, L., Liu, X., Tao, Y.T., Zhang, W. H., Chen, S. H., Meng, H., Chen, J. "XPS studies on surface reduction of tungsten oxide nanowire film by Ar+ bombardment." *Journal of Electron Spectroscopy and Related Phenomena.* 185 (3-4). pp. 112-118. 2012. DOI: 10.1016/j.elspec.2012.01.004

[23] de Angelis, B. A., Schiavello, M. "X-ray photoelectron-spectroscopy study of nonstoichio-metric tungsten-oxides." *Journal of Solid State Chemistry.* 21(1). pp. 67-72. 1977. DOI: 10.1016/0022-4596(77)90145-1

[24] Warren, A., Nylund, A., Olefjord, I. "Oxidation of tungsten and tungsten carbide in dry and humid atmospheres." *International Journal of Refractory Metals & Hard Materials.* 14 (5-6). pp. 345-353. 1996. DOI: 10.1016/s0263-4368(96)00027-3

[25] Jones, F. H., Egdell, R. G., Brown, A., Wondre, F. R. "Surface structure and spectroscopy of WO_2 (012)." *Surface Science.* 374 (1-3). pp. 80-94. 1997. DOI: 10.1016/s0039-6028(96)01219-8

[26] Hollinger, G., Pertosa, P. "Direct observation of the Anderson transition in H_xWO_3 bronzes by high-resolution X-ray photoelectron spectroscopy." *Chemical Physics Letters.* 74 (2). pp. 341-251. 1980. DOI: 10.1016/0009-2614(80)85173-6

[27] Salje, E., Carley, A. F., Roberts, M. W. "The Effect of Reduction and Temperature on the Electronic Core Levels of Tungsten and Molybdenum in WO_3 and $W_xMo_{1-x}O_3$- A Photoelectron Spectroscopic Study." *Journal of Solid State Chemistry.* 29 (2). pp. 237-251. 1979. DOI: 10.1016/0022-4596(79)90229-9

[28] Kubacka, A., Colón, G., Fernández-García, M. "Cationic (V, Mo, Nb, W) doping of TiO_2–anatase: A real alternative for visible light-driven photocatalysts." *Catalysis Today.* 143 (3-4). pp. 286-292. 2009. DOI: 10.1016/j.cattod.2008.09.028

[29] Vermaire, D. C., van Berge, P. C. "The Preparation of WO_3/TiO_2 and $WO_3/A1_2O_3$ and Characterization by Temperature-Programmed Reduction." *Journal of Catalysis.* 116 (2). pp. 309-317. 1989. DOI: 10.1016/0021-9517(89)90098-5

[30] Eibl, S., Gates, B. C., Knözinger, H. "Structure of WO_x/TiO_2 catalysts prepared from hydrous titanium oxide hydroxide: Influence of preparation parameters." *Langmuir.* 17 (1). pp. 107-115. 2001. DOI: 10.1021/la000977h

[31] Engweiler, J., Harf, J., Baiker, A. "WO_x/TiO_2 Catalysts Prepared by Grafting of Tungsten Alkoxides: Morphological Properties and Catalytic Behavior in the Selective Reduction of NO by NH_3." *Journal of Catalysis.* 159 (2). pp. 259-269. 1996. DOI: 10.1006/jcat.1996.0087

[32] Venables, D. S., Brown, M. E. "Reduction of tungsten oxides with hydrogen and with hydrogen and carbon." *Thermochimica Acta.* 285 (2). pp. 361-382. 1996. DOI: 10.1016/0040-6031(96)02951-6

[33] Micoud, F., Maillard, F., Bonnefont, A., Job, N., Chatenet, M. "The role of the support in CO_{ads} monolayer electrooxidation on Pt nanoparticles: Pt/WO_x vs. Pt/C." *Physical Chemistry Chemical Physics.* 12 (5). pp. 1182-1193. 2010. DOI: 10.1039/b915244j

[34] Ponrouch, A., Garbarino, S., Guay, D. "Effect of the nanostructure on the CO poisoning rate of platinum." *Electrochemistry Communications.* 11 (4). pp. 834-837. 2009. DOI: 10.1016/j.elecom.2009.02.006

[35] Maillard, F., Peyrelade, E., Soldo-Olivier, Y., Chatenet, M., Chaînet, E., Faure, R. "Is carbon-supported Pt-WO_x composite a CO-tolerant material?" *Electrochimica Acta.* 52 (5). pp. 1958-1967. 2007. DOI: 10.1016/j.electacta.2006.08.024

[36] Maillard, F., Schreier, S., Hanzlik, M., Savinova, E. R., Weinkauf, S., Stimming, U. "Influence of particle agglomeration on the catalytic activity of carbon-supported Pt nanoparticles in CO monolayer oxidation." *Physical Chemistry Chemical Physics.* 7 (2). pp. 385-393. 2005. DOI: 10.1039/b411377b